Facile Synthesis of Mn0.68Bi0.32OCl Mix-Crystals And Its Supercapacitive Behavior

Y.Z. Song (songyuanzhi@126.com)
Huaiyin Normal University
B.X. Qi
Huaiyin Normal University
M.T. Li
Huaiyin Normal University
J.M. Xie
Jiangsu University

Research Article

Keywords: Mn0.68Bi0.32OCl, mix-crystals, supercapacitor

Posted Date: October 26th, 2021

DOI: https://doi.org/10.21203/rs.3.rs-1004750/v1

Version of Record: A version of this preprint was published at Journal of Inorganic and Organometallic Polymers and Materials on March 18th, 2022. See the published version at https://doi.org/10.1007/s10904-022-02265-5.

Abstract

$Mn_{0.68}Bi_{0.32}OCl$ mix-crystals for supercapacitor were successfully synthesized via a facile solid-phase method using $Bi(NO_3)_3$ and $MnCl_2$ with molar ratio of 1:1 as precursors. The $Mn_{0.68}Bi_{0.32}OCl$ mix-crystals were characterized by scanning electron microscopy, X-ray diffraction, Brunauer-Emmett-Teller surface area measurements and thermogravimetry and differential scanning calorimetry, respectively. Cyclic voltammetry and galvanostatic charge/discharge technique were performed for the $Mn_{0.68}Bi_{0.32}OCl$ mix-crystals in 1 M Na_2SO_4 aqueous solutions; the specific capacitance of $Mn_{0.68}Bi_{0.32}OCl$ was about 203 $F.g^{-1}$ at the current density of 3 A. g^{-1} with a long life time, owing to the high power density of $Mn_{0.68}Bi_{0.32}OCl$ mix-crystals and the higher surface area, good conductivity, and high stability of the $Mn_{0.68}Bi_{0.32}OCl$ mix-crystals.

1. Introduction

Supercapacitor as a next generation of promising electrochemical energy storage device has the advantages of fast charge and discharge speed, long service life, high power density, high safety and good cycle stability. Based on the charge storage mechanism, supercapacitors can be divided into double-layer capacitors, pseudo capacitors and hybrid supercapacitors. The two-layer capacitor consists of activated carbon electrode material, and pseudocapacitive supercapacitors include metal oxide electrode materials and polymer electrode materials. Mn and Bi are environmentally friendly and inexpensive, widely used in the preparation of supercapacitors, and the Mn_3O_4 [1], MnO [2], MnOx [3], Mn_2O_3 [4], Bi_2O_3 [5–8], BiOCl [9], (Cu)BiOCl [10], and BiOBr [11] supercapacitors have been prepared for supercapacitors.

BiOCl as a semiconductor material was often widely used in the field of photocatalysis [12–13] due to its special layered structure, which is composed of $[Bi_2O_2]^{2+}$ layer and double-layer halogen ion layer staggered along the [001] direction, and its synthesis mainly include hydrothermal / solvothermal method, template method, ultrasonic method, solid-phase method and sol-gel method [14–19]. The band gap of BiOCl is 3.6 eV, the ion doping was a effective for improving the catalytic performance of BiOCl [20], the different molar ratio manganese-doped BiOCl composites (Mn/BiClO) were prepared using Bi $(NO_3)_3$ and $Mn(CH_3COO)_2$ as precursors by the hydrothermal method with imidazole hydrochloride [HMIM]Cl as the chlorine source and template for the photocatalytic degradation of rhodamine [21], Cao et al. synthesized the Mn^{3+} doping BiOCl in hydrochloric acid and potassium chloride solution using Bi $(NO_3)_3$ and $MnCl_2$ with molar ratio of 1:0.015 as the precursors by hydrothermal method for the metronidazole photodegradation [22], the Bi(Mn)OCl could also be synthesized using hydrothermal method by adjusting the pH of $MnCl_2$-$BiCl_3$-HCl solution with ammonia water for the degradation of malachite green dye [23].

In present work, the $Mn_{0.68}Bi_{0.32}OCl$ was synthesized in one step using Bi $(NO_3)_3$ and $MnCl_2$ with molar ratio of 1:1 as precursors by hot solid phase method, the material was characterized by spectroscopy and

electrochemistry, and its supercapacitive behavior was studied.

2. Experimental

2.1. Materials

60% polyvinylidene fluoride (PVDF) water emulsion was provided by Shanghai San-Ai-Fu new material Ltd (Shanghai, China). N. N-dimethylformamide, Na_2SO_4, Bi $(NO_3)_3.5H_2O$ and $MnCl_2.4H_2O$ were purchased from from Shanghai Analytical Chemicals Company. All chemicals were of analytical grade without further purification. Graphite electrode was used as active material carrier because of its low price, good adsorb ability and electrochemical stability. At the same time, graphite was easy to make flexible electrode. The graphite electrode was prepared by the following method: the graphite electrode of a diameter of 14.0 mm was inserted into the polypropylene-random (PPR) plastic pipe of an inner diameter of 14.00 mm, the surface of graphite electrode was polished using sandpaper of 1000 and 7000 mesh to the mirror, respectively, then further cleaned with polishing cloth, and the other end was connected the with a copper column. The prepared graphite electrode was sonicated with deionized water and ethanol for 30 minutes, respectively, and dried for standby.

2.2. Synthesis of $Mn_{0.68}Bi_{0.32}OCl$

0.01M Bi $(NO_3)_3.5H_2O$ and $MnCl_2.4H_2O$ were dissolved with 0.01 M HNO_3 of 30 ml in a porcelain crucible and heated in a 100 ℃ oven for 24 hours for nearly dry, then the mixture was transferred into a muffle furnace, heated from room temperature to 500 ℃for 0.5 h, kept at 500 ℃ for 4 h, from 500 to 600 ℃ for 0.5 h, kept 600 ℃ for 1 h, and cooled to room temperature for use.

2.3. Material characterization

The nitrogen adsorption and desorption experiments of $Mn_{0.68}Bi_{0.32}OCl$ were carried out at 77 K using SA3100 surface area and pore size analyzers (Beckman Coulter, Inc. USA). The morphologies of $Mn_{0.68}Bi_{0.32}OCl$ were examined by scanning electron microscope (SEM) (QUANTA FEG 450, USA), equipped with an EDAX OCTANE PRO energy dispersive spectrometer (EDS) (FEI, USA). The thermogravimetry (TG) and differential scanning calorimetry (DSC) were performed using a NETZSCH STA 449F3 simultaneous thermal analyzer (German). X-Ray diffraction (XRD) analysis was performed on the $Mn_{0.68}Bi_{0.32}OCl$ with a Switzerland ARL X'TRA X-ray diffractometer rotating anode with Cu-Kα radiation source (λ = 0.1540562 nm).

2.4. Electrochemical characterization

To investigate the supercapacitive behavior of the nanomix-crystals, the active material, carbon black (CB) and PVDF were taken in the weight ratios of 100 : 10 : 10. The mixture of $Mn_{0.68}Bi_{0.32}OCl$ of 10.0 mg, CB of 1.0 mg and PVDF of 1.0 mg was firstly dispersed in N. N-dimethylformamide of 10.00 ml, ultrasound for 30 minutes, then the mixture of 100 μl evenly dispersed on the surface of the clean graphite electrode, and finally dried at 100℃ for 1 h. The loading mass of active material was 0.10 mg.

Land-CT2001A battery analyzer (Wuhan, China) was utilized for the charge/discharge cycling life tests of $Mn_{0.68}Bi_{0.32}OCl$. The electrochemical characterization of the prepared capacitive electrodes was also carried out with a CHI660e electrochemical analyzer (CHI, USA) in a three-electrode cell system. The prepared capacitive electrode was used as working electrode, a about 0.80 cm graphite rod in diameter of 1.40 cm were counter and reference electrodes, and the length of reference graphite electrode was selected according to the equal electric quantity of charge and discharge curve. The electrochemical impedance spectroscopy (EIS) was measured at the open-circuit potential over the frequency range of 0.02 to 10^5 Hz with an a.c. amplitude of 5 mV. All electrochemical measurements were carried out at room temperature.

3. Results And Discussion

3.1 Specific surface area of $Mn_{0.68}Bi_{0.32}OCl$

As shown in Fig. 1, the isotherm of $Mn_{0.68}Bi_{0.32}OCl$ was classified as type IV with an H3 hysteresis loop. The specific surface area (SSA) was calculated using the Brunauer Emmett-Teller (BET) method. The pore-size distributions (PSDs) of $Mn_{0.68}Bi_{0.32}OCl$ were also computed by the Barrett Joyner Halenda (BJH) plots. The peak in PSDs (shown in Fig. 1 inset) was centered at 37.3 and 242.2 nm. The SSA values of $Mn_{0.68}Bi_{0.32}OCl$ calculated by BET method were 14.6 $m^2\ g^{-1}$, which was more than 13.28 $m^2\ g^{-1}$ of Mn-doped BiOCl [22], and conducive to the penetration of electrolyte into the surface of electroactive substances.

3.2 Micrographs and EDS spectrum of $Mn_{0.68}Bi_{0.32}OCl$

The SEM micrographs and the EDS spectrum of $Mn_{0.68}Bi_{0.32}OCl$ are shown in Fig. 2 and Fig. 3, respectively. The SEM micrographs in Fig. 2 showed that the smooth surface, neat edges and layered particles could be ascribed to the Bi (Mn) OCl mix-crystals. The EDS measurements in Fig. 3 further demonstrated the chemical composition of products. The EDS spectra and element analysis revealed that the rate of O : (Mn+ Bi) : Cl was 1.42 : 0.73 : 1, while the rate of Mn: Bi was 2.09 : 1. From Table 1 the measurement errors of O and Cl elements were more than those of Mn and Bi elements, suggesting that the chemical formula of the so-prepared product was $Mn_{0.68}Bi_{0.32}OCl$.

The reaction mechanism should be as follows: The Bi^{3+} in the dilute nitric acid was hydrolyzed to $BiONO_3$, then which was substituted by the Mn^{2+} and Cl^-. The sublimation temperatures of $MnCl_2$ and $BiCl_3$ are 1190 and 430°C, respectively [24], respectively, so the product contained less Bi. The reaction equations were given as

$$Bi(NO_3)_3+H_2O\rightarrow BiONO_3\downarrow+2HNO_3$$

$$BiONO_3+MnCl_2+O_2\rightarrow Mn_{0.68}Bi_{0.32}OCl+BiCl_3\uparrow+NO_3^-$$

$$4HNO_3\rightarrow 4NO_2\uparrow+2H_2O+O_2\uparrow$$

Table 1
Elemental analysis of $Mn_{0.68}Bi_{0.32}OCl$

Element	Weight%	Atom%	Intensity	Error %
O K	16.97	45.29	14.08	14.59
BiM	36.67	7.49	79.66	3.69
ClK	26.20	31.56	41.75	11.46
MnK	20.16	15.67	34.52	4.23

3.3 XRD pattern of $Mn_{0.68}Bi_{0.32}OCl$

The XRD pattern of $Mn_{0.68}Bi_{0.32}OCl$ is shown in Fig. 4. The diffraction peaks of $Mn_{0.68}Bi_{0.32}OCl$ matched well with the structure of BiOCl (PDF#85-0861), the peaks of 12.14 º, 24.28 º, 25.99 º, 32.63 º, 33.58 º, 36.68 º, 41.02 º, 46.78 º, 49.56 º, 49.83 º, 54.20 º, 55.24 º, 58.74 º, 60.51 º, 60.78 º, 63.15 º, 68.19 º, 69.59 º, 75.09 º, 77.62 º, 77.82º could be assigned to the diffraction plane of (001), (002), (101), (110), (102), (003), (112), (200), (004), (113), (211), (10 4), (212), (114), (203), (005), (220), (221), (214), (310) and (302), respectively, the (001) peak of the $Mn_{0.68}Bi_{0.32}OCl$ showed a clear shift of ~0.112 º to the right compared to the BiOCl, and no other impurity peaks were found, demonstrating that the Bi^{3+} ions of BiOCl were easy to be replaced by Mn^{3+} ions to produce mix-crystal $Mn_{0.68}Bi_{0.32}OCl$.

3.4 TG and DSC of $Mn_{0.68}Bi_{0.32}OCl$

The TG and DSC curves of $Mn_{0.68}Bi_{0.32}OCl$ are shown in Fig. 5. When the temperature raised to 700 ℃, the mass of sample increased by about 1.8 %, which could be attributed to the oxidation of MnOCl on the surface of $Mn_{0.68}Bi_{0.32}OCl$ to Mn_2O_3 due to the stable Mn_2O_3 [25, 26]; when the temperature raised from 832 ℃ the mass of 86.8 % was remained, and the mass in the temperature range of 832 to 898 ℃ slowly decreased to 86.0%, which could be attributed to the oxidative decomposition of $Mn_{0.68}Bi_{0.32}OCl$ into Mn_2O_3, Bi_2O_3, and $BiCl_3$ [27] because BiOCl was steady below 600°C [13], while when the temperature reaches 1000 ℃ the mass of 79.3 % was remained, reveling that $Mn_{0.68}Bi_{0.32}OCl$ was a higher safe material.

3.5. Electrochemical performance of $Mn_{0.68}Bi_{0.32}OCl$

The electrochemical performance of $Mn_{0.68}Bi_{0.32}OCl$ was examined with cyclic voltammetry (CV) in Fig. 6 and galvanostatic charge/discharge in 1 M Na_2SO_4 aqueous solutions in a fixed voltage window of -0.50 ~ 0.50 V vs. graphite in Fig. 7. From Fig. 6(a) it could be seen that the oxidation current increased with the increase of voltage, and a oxidation peak was found at 2.556 V, which could be attributed to Mn^{3+} / Mn^{4+}, indicating that the change of electrode potential in the range of -0.5 ~ 0.5 V mainly came from the diffusion of ions, and the electrode of $Mn_{0.68}Bi_{0.32}OCl$ with the richer O and Cl elements of higher electronegativity, had higher adsorption capacity for the Na^+ ions. Fig. 6(b) indicated that the electrodes in the range of -0.5 ~ 0.5 V had the characteristics of supercapacitor at low sweep speed.

The galvanostatic charge/discharge curves are shown in Fig. 7. The specific capacitance (SC) value was calculated by the formula as$SC = \frac{it}{m\Delta V}$. The SC value of $Mn_{0.68}Bi_{0.32}OCl$ electrode (WE) at current density of 3, 5, 7, and 10 A g^{-1} was 113.9, 63.0, 23.0 and 7.7 F g^{-1}, respectively, which was significantly affected by the current density. Compared with the bare electrode (BE) and the CBE (working electrode of absent $Mn_{0.68}Bi_{0.32}OCl$), an SC value of 5.8 F g^{-1} for the BE and 9.0 F g^{-1} for the CBE at the current density of 3 A g^{-1} was less than that of the WE, revealing that the capacitance was mainly derived from the $Mn_{0.68}Bi_{0.32}OCl$.

The cycling stabilities of $Mn_{0.68}Bi_{0.32}OCl$ were evaluated at a current density of 3 A g^{-1} for 10000 cycles in Fig. 8. From Fig. 8 the SC values from cycle 1 to 12 at the current density of 3 A g^{-1} increased due to the penetration of electrolyte into electrode active material, and the SC value of the first cycle was 124.2 F g^{-1} at the current density of 3 A g^{-1}, which was close to the value of 113.9 F g^{-1} obtained with CHI660e electrochemical analyzer. And from cycle 13 to 10000 the SC values at the current density of 3 A g^{-1} were in the range of 211.8 ~ 224.0 F g^{-1} with cycle efficiencies (n%) of 94.5 ~ 106.0 %, indicating that the electrode materials had higher stability.

The EIS analysis was also used to predict the behavior of the capacitive electrode. As shown in Fig. 9 the Faradic charge transfer resistances (R_{ct}) corresponding to the diameter of the semicircle in the plot, were closely related to the surface area and conductivity of the electrode, and the straight sloping line was associated with the ions diffusion. And the intercepts of BE, CBE, and WE in the Nyquist plots, which were related to the electrical resistance of the electrolyte (R_{ele}), were about 0.53, 0.79, 4.64 Ω with smaller R_{ct}, indicating that the electrolyte ions easily accessed the surface of active material, and the electroactive material on the electrode had stronger depolarization ability, which could promote the transfer of ions and electrons. Also, the slope of ions diffusion was steeper, demonstrating that $Mn_{0.68}Bi_{0.32}OCl$ had faster diffusion of electrolyte ions.

4. Conclusions

In this paper the $Mn_{0.68}Bi_{0.32}OCl$ were prepared using Bi $(NO_3)_3$ and $MnCl_2$ of molar ratio of 2:1 as precursors by hot solid phase method. The $Mn_{0.68}Bi_{0.32}OCl$ with simple preparation and low cost showed

a distinctly improved electrochemical performance of supercapacitor because of the high SSA, good electrical conductivity and absorption and perfect stable crystallinity of $Mn_{0.68}Bi_{0.32}OCl$. The improved rate performance and good cycling stability make it as a promising electrode material for supercapacitor.

Declarations

Acknowledgment

The authors gratefully acknowledge the financial support of the Open Science Foundation for Jiangsu Province Key Laboratory for Chemistry of Low-Dimentional Materials (grant no. JSKC11091), the Open Science Foundation for Jiangsu Key Laboratory for Biomass–based Energy and Enzyme Technology (grant no. JSBEET1207), and the Science foundation for Huaiyin Normal University (grant no.11HSGJBZ13).

References

1. H. Wu, D. He, Y. Wang, Facile one-step process synthesized reduced graphene oxide/Mn3O4 nanocomposite for a symmetric supercapacitor. Mater. Lett. **268**, 127613(2020).

2. Y. Zhou, X. Cheng, B. Tynan, Z. Sha, F. Huang, M. S. Islam, J. Zhang, A. N. Rider, L. Dai, D. Chu, D. Wang, Z. Han, C. Wang, High-performance hierarchical MnO_2/CNT electrode for multifunctional supercapacitors. Carbon **184**, 504-513(2021).

3. H. Zhou, Y. Zhan, F. Guo, S. Du, B. Tian, Y. Dong, L. Qian, Synthesis of biomass-derived carbon aerogel/MnOx composite as electrode material for high-performance supercapacitors. Electrochim. Acta **390**, 138817 (2021).

4. Y. Chen, R. Yang, C. Chen, Y. Li, M. Wei, Construction of hierarchical Mn_2O_3 hollow microspheres derived from metal–organic frameworks for high performance supercapacitors. J. Power Sources 505, 230077(2021).

5. M. Pooladi, M. M. Zerafat, Controlled micro/mesoporous carbon aerogel structure as a template for Bi_2O_3 nano-particles/rods to improve the performance of asymmetric supercapacitors. J. Energy Storage **42**, 102994 (2021).

6. R. Yi, R. Wang, J. Duan, Z. Fang, H. Li, Z. Chen, A. Zhou, Y. Sun, Rational design of hierarchically porous $NiCo_2O_4$ and Bi_2O_3 nanostructure: Anchored on 3D nitrogen doped carbonized melamine foam for flexible asymmetric supercapacitor. Electrochim. Acta **338**, 135845(2020).

7. H. Wu, J. Guo, D. Yang, Facile autoreduction synthesis of core-shell Bi-Bi_2O_3/CNT with 3-dimensional neural network structure for high-rate performance supercapacitor. J. Mater. Sci. Technol. **47**, 169–176(2020).

8. A. Deepi, G. Srikesh, A. Samson Nesaraj, Electrochemical performance of Bi_2O_3 decorated graphene nano composites for supercapacitor applications. Nano-Structures & Nano-Objects **15**, 10–16(2018).

9. S. Dutta, S. Pal, D. Sikder, S. De, Light-weight flexible solid-state supercapacitor based on highly crystalline 2D BiOCl nanoplates/MWCNT nanocomposites. J. Alloy. an Compd. **820**, 153115(2020).

10. R. Rameshbabua, M. Sandhiya, Gina Pecchi, M. Sathish, Effective coupling of Cu (II) with BiOCl nanosheets for high performance electrochemical supercapacitor and enhanced photocatalytic applications. Appl. Surf. Sci. **521**, 146362 (2020).

11. H. Tian, R. Cheng, M. Lin, P. Li, Y. Lv, S. Ranc, Oxygen-vacancy-rich ultrathin BiOBr nonosheets for high-performance supercapacitor electrodes. Inorg. Chem. Commun. **118**, 108018 (2020).

12. Y. Li, Y. Zhao, G. Wu, H. Ma, J. Zhao, Bi superlattice nanopolygons at BiOCl (001) nanosheet assembled architectures for visible-light photocatalysis, Mater. Res. Bull. **101**, 39–47(2018).

13. Z. SHI, Y. WANG, C. FAN, Y. WANG, G. DING, Preparation and photocatalytic activity of BiOCl catalyst. Trans. Nonferrous Met. Soc. China **21**, 2254–2258(2011).

14. K. Zhao, L. Zhang, J. Wang, Q. Li, W. He, J. J. Yin, Surface structure-dependent molecular oxygen activation of BiOCl single-crystalline nanosheets. J. Am Chem Soc. **135**,15750-15753(2013).

15. X. Zhang, X. Wang, L. Wang, W. Wang, L. Long, W. Li, H. Yu, Synthesis of a highly efficient BiOCl single-crystal nanodisk photocatalyst with exposing {001} facets. ACS Appl. Mater. Inter. **6**: 7766(2014).

16. L. Suryanti, S.E.I. S. Hartatiek, Nasikhudin, J. Utomo, A. Taufiq, R. Suryana, Z. Aspanutd, M. Diantoro, The effect of Mn_2O_3 nanoparticles on its specific capacitance of symmetric supercapacitors FC-ZnO-x(Mn_2O_3). Mater. Today: Proc. **44**, 3355–3360(2021)

17. C. Wang, X. Zhang, H. Qiu, W. Wang, G. Huang, J. Jiang, H. Yu, Photocatalytic degradation of bisphenol by oxygen-rich and highly visible-light responsive $Bi_{12}O_{17}C_{l2}$ nanobelts. Appl. Catal. B Environ. **200**, 659-665(2017).

18. Y. Tian, C. F. Guo, Y. Guo, Q. Wang, Q. Liu, BiOCl nanowire with hierarchical structure and its Raman features. Appl. Surf. Sci. **258**, 1949-1954 (2012).

19. Y. Zhang, M. Park, H. Kim, Soo-Jin. Park, In-situ synthesis of graphene oxide/BiOCl heterostructured nanofibers for visible-light photocatalytic investigation. J.Alloy. Compd. **686**, 106-114(2016).

20. T. Zhang, L. Chen, T. Jiang, J. Hou, G. Zhang, A. Hussain, Chemical precipitation synthesis of $Bi_{0.7}Fe_{0.3}OCl$ nanosheets via Fe (III)-doped BiOCl for highly visible light photocatalytic performance. Mater. Today Commun. **26**, 102145 (2021).

21. R. Zhao, X. Li, K. Lin, X. Gao, Preparation and photocatalytic performance of the Mn/ BiOCl albizia flower. Res Chem Intermed **42**, 7031–7043 (2016).

22. J. Cao, J. Li, W. Chua, W. Cen, Facile synthesis of Mn-doped BiOCl for metronidazole photodegradation: Optimization, degradation pathway, and mechanism. Chem. Eng. J. **400**, 125813 (2020).

23. B. Pare, B. Sarwan, S. B. Jonnalagadda, Photocatalytic mineralization study of malachite green on the surface of Mn-doped BiOCl activated by visible light under ambient condition. Appl. Surf. Sci. **258**, 247–253 (2011).

24. https://www.chemicalbook.com

25. M. Karuppaiah, P. Sakthivel, S. Asaithambi, R. Murugan, G. Anandhababu, R. Yuvakkumar, G. Ravi, Solvent dependent morphological modification of micro-nano assembledMn_2O_3/NiO composites for high performance supercapacitor applications. Ceram. Int.**45**, 4298–4307(2019).

26. Ao. Wang, P. Huang, P. Sun, F. Shi, B. Tian, J. Gao, Synthesis and crystal structure of a Mn-based coordination complex asprecursor for the synthesis of Mn_2O_3. . Chim. Acta **498**, 119166(2019).

27. P. Zhou, Y. Shen, S. Zhao, G. Li, B. Cui, D. Wei, Y. Shen, Synthesis of clinoptilolite-supported BiOCl/TiO_2 heterojunction nanocomposites with highly-enhanced photocatalytic activity for the complete degradation of xanthates under visible light.Chem. Eng. J. 407, 126697(2021).

Figures

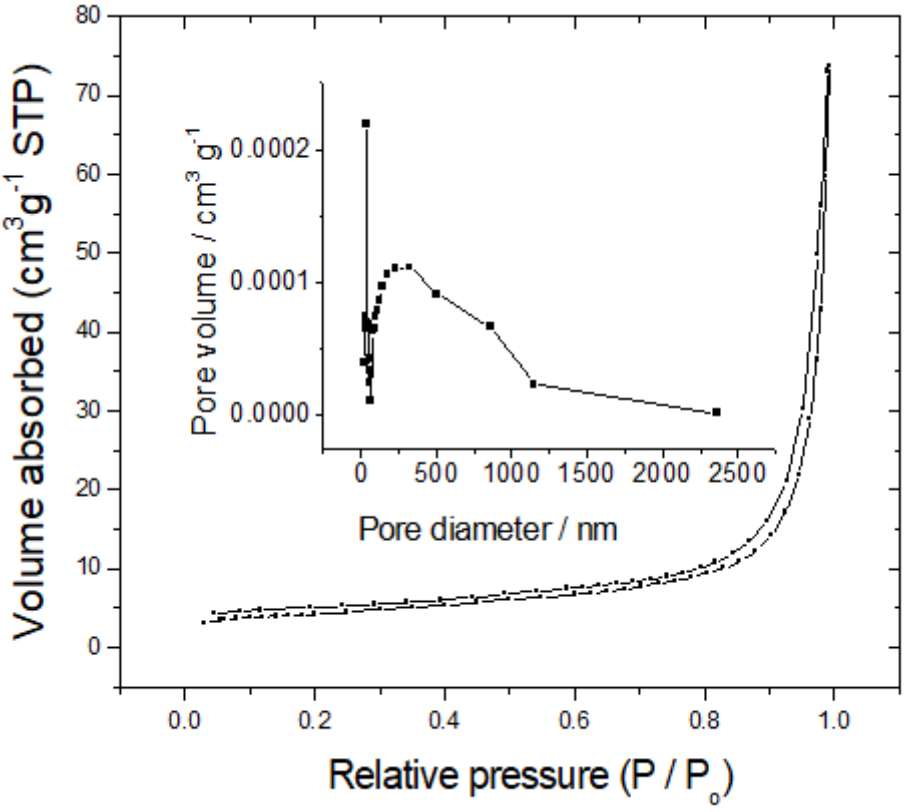

Figure 1

Nitrogen adsorption/desorption isotherms and BJH pore-size distribution of curves (inset) of Mn0.68Bi0.32OCl

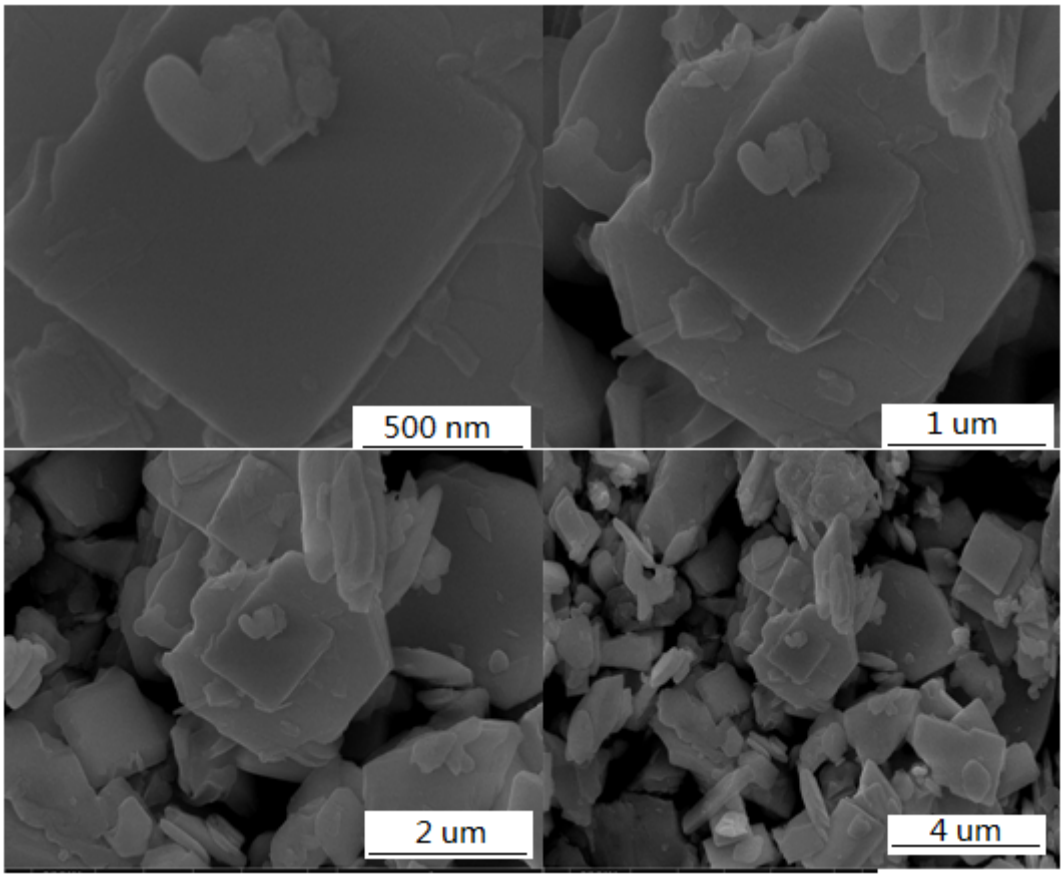

Figure 2

SEM images of Mn0.68Bi0.32OCl.

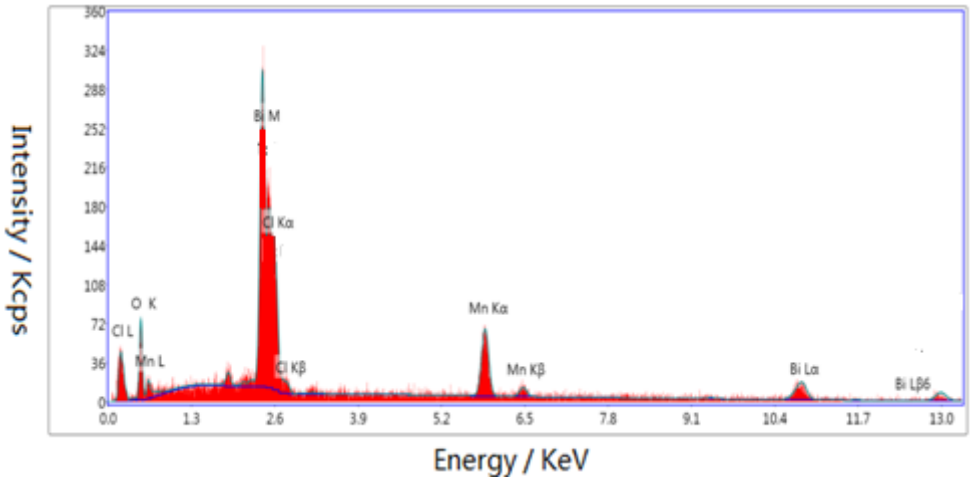

Figure 3

EDS spectra of Mn0.68Bi0.32OCl

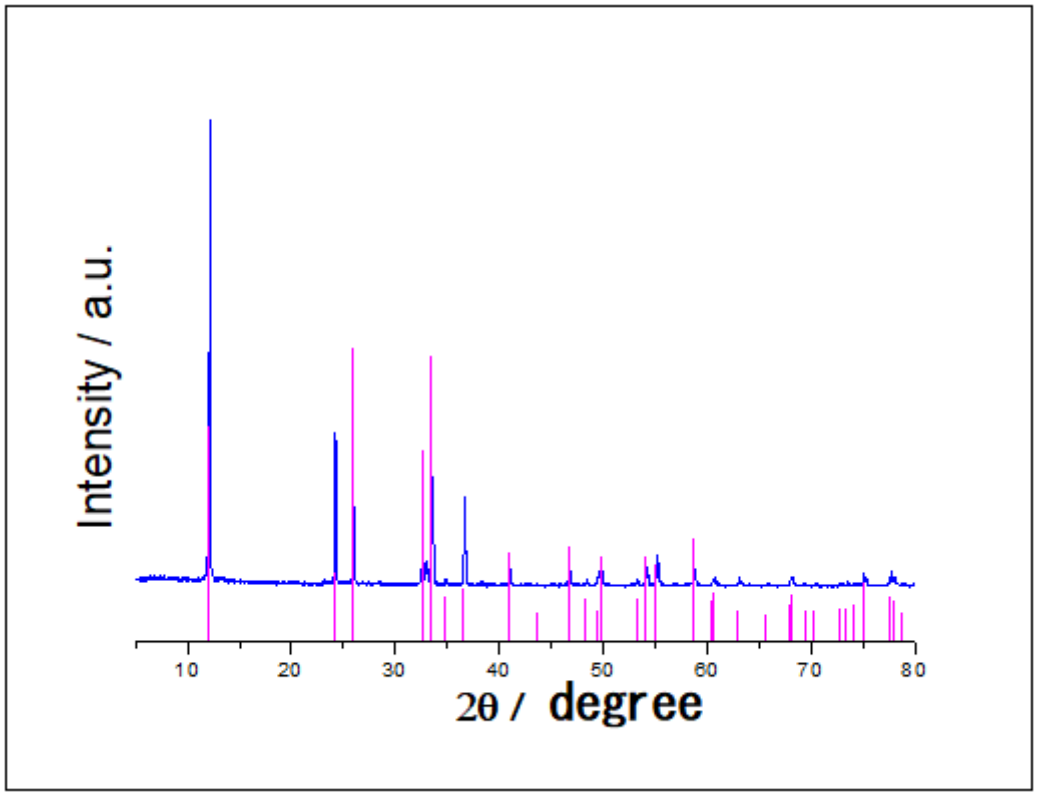

Figure 4

XRD pattern of Mn0.68Bi0.32OCl(a) and BiOCl (b)

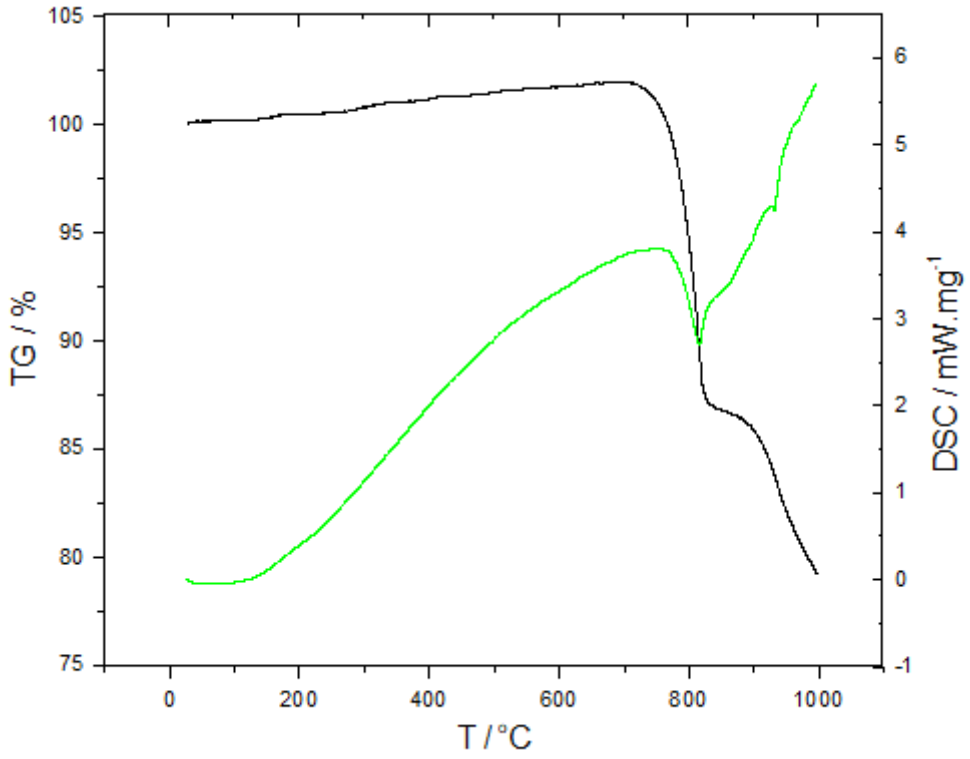

Figure 5

TG (a) and DSC (b) curves of Mn0.68Bi0.32OCl

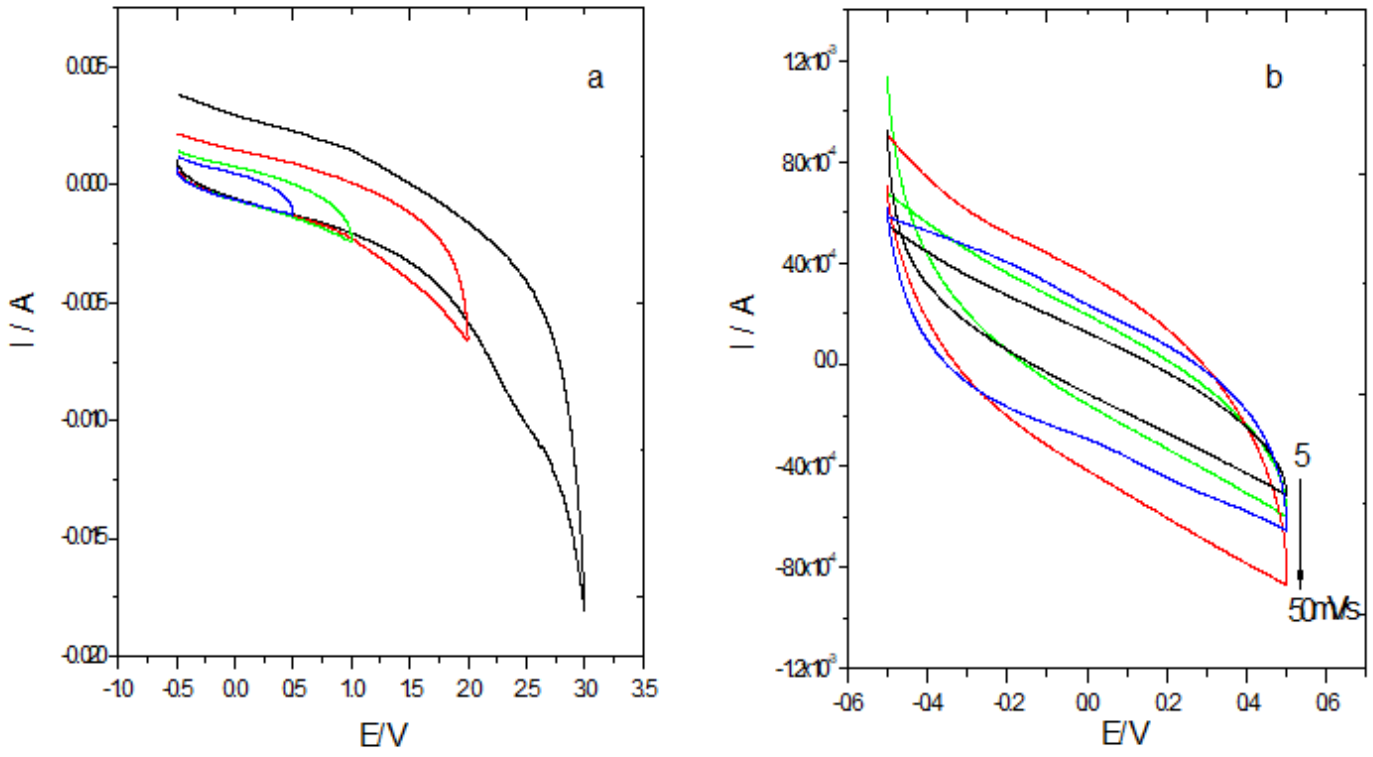

Figure 6

Cvs of Mn0.68Bi0.32OCl at different voltage window (a) and scan rate of 5, 10, 30, and 50 mV s-1(b).

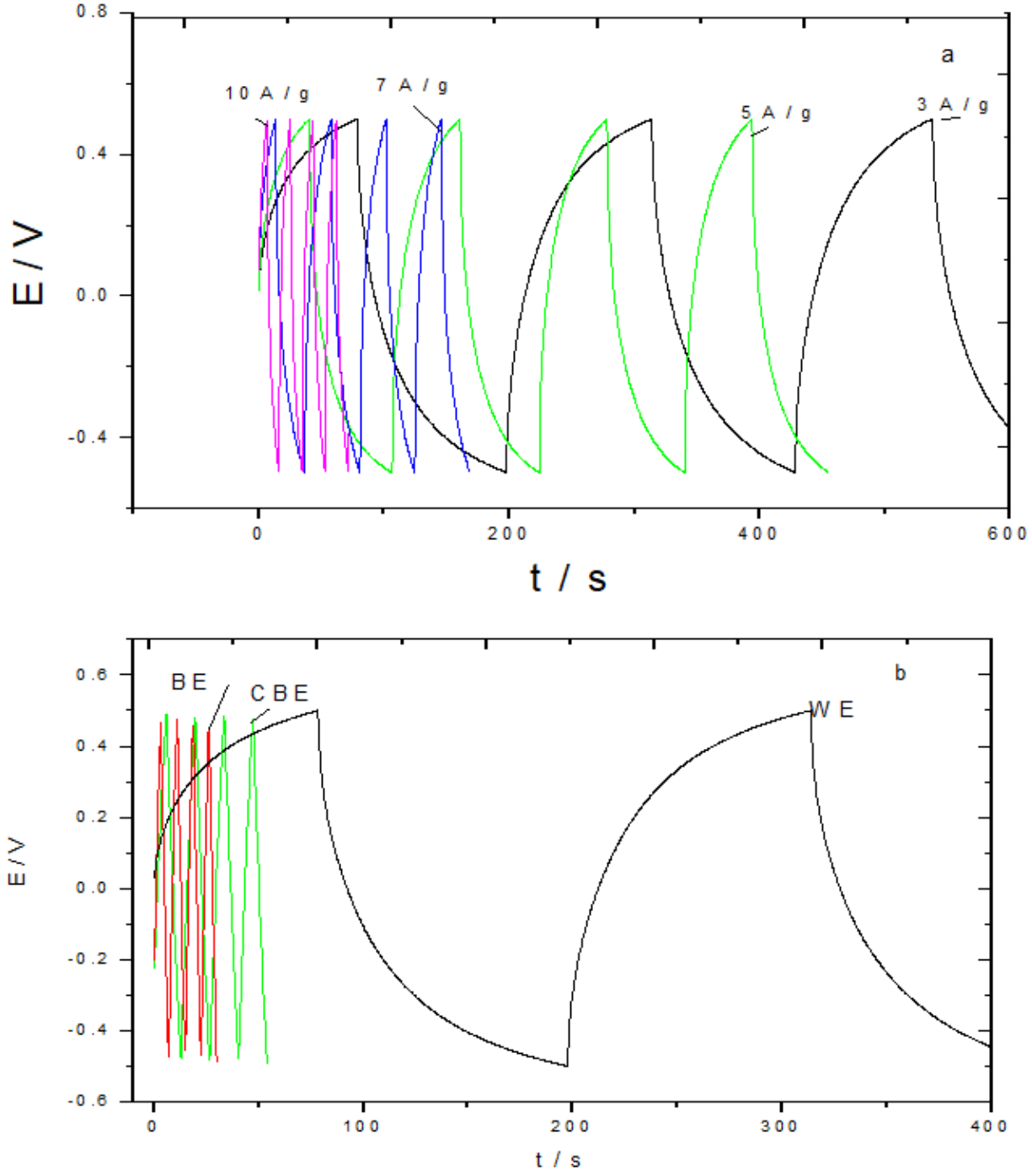

Figure 7

Galvanostatic charge/discharge curves of WE at the current density of 3 □ 10A g-1 (a) and compared electrode at the current density of 1 A g-1 (b).

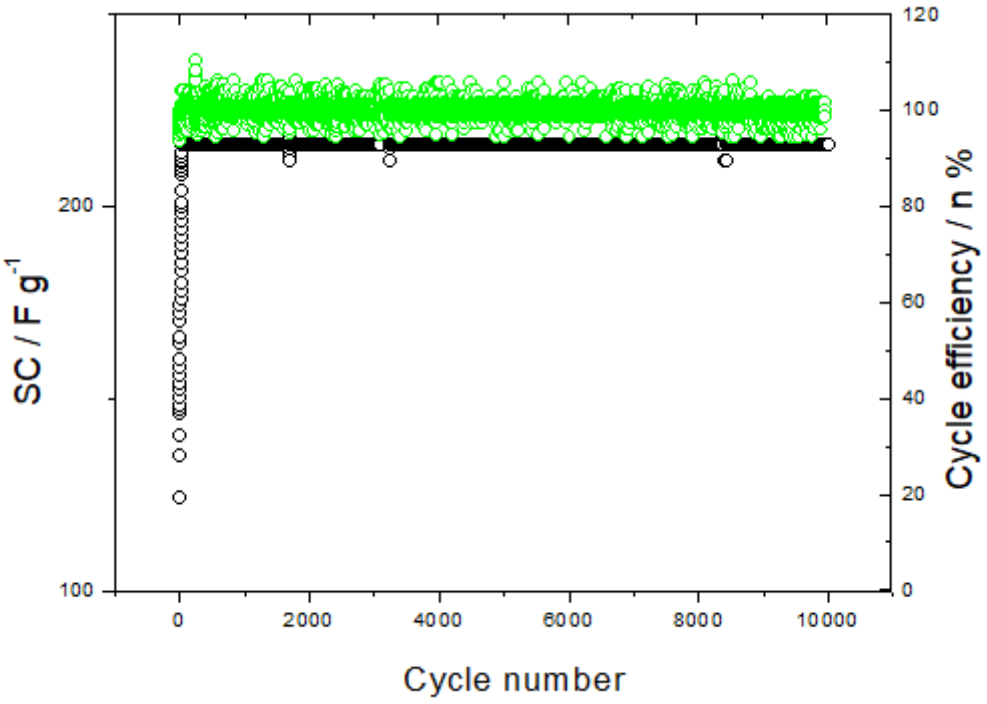

Figure 8

Plot of variation in the SC values of Mn0.68Bi0.32OCl at a current density of 3 A g-1

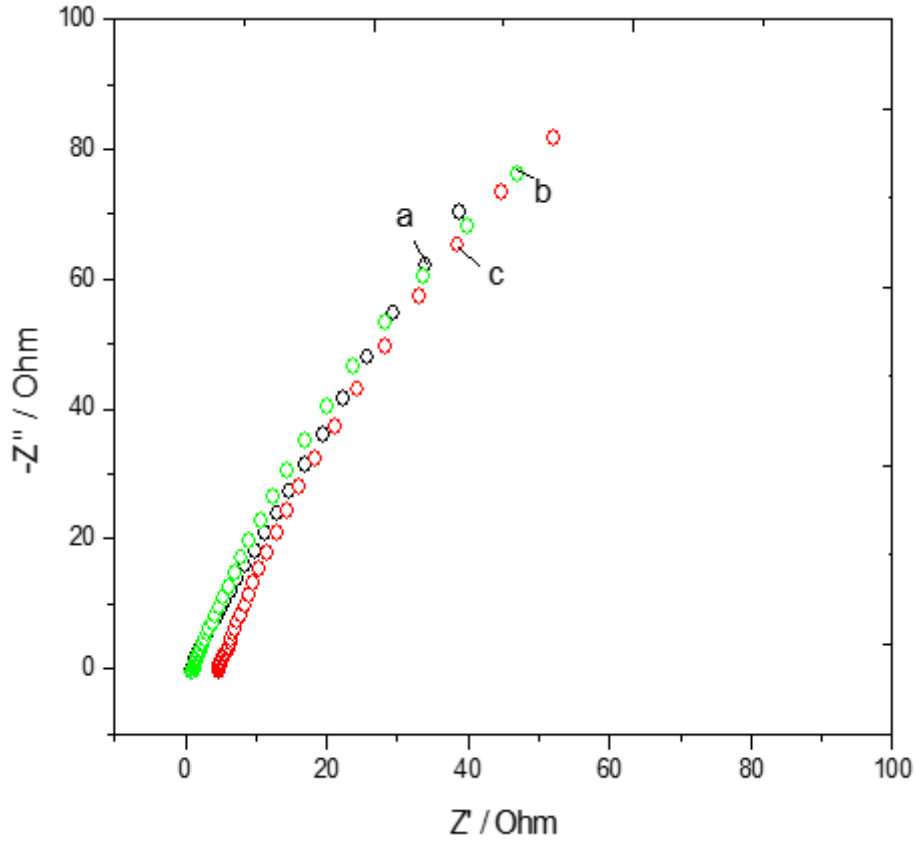

Figure 9

EIS of Mn0.68Bi0.32OCl (a: BE; b: CBE; c: WE)